

The $^{13}\text{N}(d, n)^{14}\text{O}$ Reaction and the Astrophysical $^{13}\text{N}(p, \gamma)^{14}\text{O}$ Reaction Rate

Z. H. Li,* B. Guo, S. Q. Yan, G. Lian, X. X. Bai, Y. B. Wang, S. Zeng, J. Su,
B. X. Wang, W. P. Liu, N. C. Shu, Y. S. Chen, H. W. Chang, and L. Y. Jiang
China Institute of Atomic Energy, P. O. Box 275(46), Beijing 102 413, P. R. China

Abstract

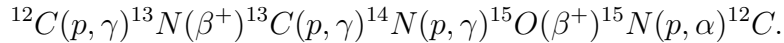
$^{13}\text{N}(p, \gamma)^{14}\text{O}$ is one of the key reactions in the hot CNO cycle which occurs at stellar temperatures around $T_9 \geq 0.1$. Up to now, some uncertainties still exist for the direct capture component in this reaction, thus an independent measurement is of importance. In present work, the angular distribution of the $^{13}\text{N}(d, n)^{14}\text{O}$ reaction at $E_{\text{c.m.}} = 8.9$ MeV has been measured in inverse kinematics, for the first time. Based on the distorted wave Born approximation (DWBA) analysis, the nuclear asymptotic normalization coefficient (ANC), $C_{1,1/2}^{14\text{O}}$, for the ground state of $^{14}\text{O} \rightarrow ^{13}\text{N} + p$ is derived to be 5.42 ± 0.48 fm $^{-1/2}$. The $^{13}\text{N}(p, \gamma)^{14}\text{O}$ reaction is analyzed with the R-matrix approach, its astrophysical S-factors and reaction rates at energies of astrophysical relevance are then determined with the ANC. The implications of the present reaction rates on the evolution of novae are then discussed with the reaction network calculations.

PACS numbers: 21.10.Jx, 25.40.Lw, 25.60.Je, 26.30.+k

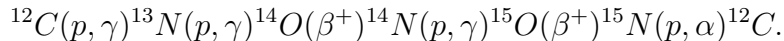
*Electronic address: zhli@ciae.ac.cn

I. INTRODUCTION

In stellar-evolution models, hydrogen burning in massive stars proceeds largely through the CNO cycle. For the normal CNO cycle, the dominant sequence of reactions is



When temperature increases, the β^+ decay of ^{13}N limits the cycle, and most of the C, N and O nuclei would be processed into ^{13}N . Consequently, the $^{13}\text{N}(p, \gamma)^{14}\text{O}$ reaction provides a second channel for destruction of ^{13}N , and the dominant sequence becomes



This reaction sequence is called hot or “ β -limited” CNO cycle, and the β^+ decays of ^{14}O and ^{15}O limit this cycle. The CNO cycles convert four hydrogen nuclei into an alpha particle and the energy release in the cycles is about 26.7 MeV, which is the important source of stellar energy generation [1]. Since the β^+ decays of ^{14}O and ^{15}O are much quicker than that of ^{13}N , the hot CNO cycle should produce energy much faster than the normal CNO cycle. Hence, a rapid change of the temperature dependent energy generation rate occurs when the CNO cycle transits from the normal one to the hot one. $^{13}\text{N}(p, \gamma)^{14}\text{O}$ is one of the important reactions which controls this transition [2]. Therefore precise determination of the rates for the ^{13}N proton capture reaction is vital for determining the transition temperature and density between the normal and hot CNO cycles.

At the energies of astrophysical interest, the $^{13}\text{N}(p, \gamma)^{14}\text{O}$ reaction is dominated by the low energy tail of the s -wave capture on the broad 1^- resonance at $E_r = 527.9$ keV (which has a total width of 37.3 ± 0.9 keV). A considerable effort has been expended in recent years to determine the parameters for the resonance. These include the direct measurements using the radioactive ^{13}N beam [3, 4], particle transfer reactions [5, 6, 7, 8], and Coulomb dissociation of high-energy ^{14}O beams in the field of a heavy nucleus [9, 10, 11]. The direct capture contribution is significantly smaller than the contribution due to the tail of the resonance within the Gamow window. But since both resonant and non-resonant captures proceed via s -waves and then decay by E1 transitions, there is an interference between the two components. Thus the capture reaction within the Gamow window can be enhanced through constructive interference or reduced through destructive interference.

The non-resonant component of the cross section has been calculated by several groups, either separately or as part of the calculation of the total cross section [1, 12, 13, 14]. Since there are significant differences among the various calculations, the determination of the $^{13}\text{N}(p, \gamma)^{14}\text{O}$ direct capture component through an independent approach is greatly needed. A practicable method is to extract the direct capture cross section of the $^{13}\text{N}(p, \gamma)^{14}\text{O}$ reaction using the direct capture model [15, 16] and the spectroscopic factor (or ANC), which can be deduced from the angular distribution of one proton transfer reaction. Decroock et al. extracted the spectroscopic factor for $^{14}\text{O} \rightarrow ^{13}\text{N} + p$ from the $^{13}\text{N}(d, n)^{14}\text{O}$ cross section [17]. Tang et al. derived the ANC for $^{14}\text{O} \rightarrow ^{13}\text{N} + p$ from the $^{14}\text{N}(^{13}\text{N}, ^{14}\text{O})^{13}\text{C}$ angular distribution [18]. The S-factors for the direct capture of the $^{13}\text{N}(p, \gamma)^{14}\text{O}$ reaction from these two works differ from each other by a factor of 30%. Thus, further measurement is important for the determination of the spectroscopic factor (or ANC) for $^{14}\text{O} \rightarrow ^{13}\text{N} + p$ and the astrophysical S-factor of the $^{13}\text{N}(p, \gamma)^{14}\text{O}$ reaction.

In the present work, we have measured the angular distribution of the $^{13}\text{N}(d, n)^{14}\text{O}$ reaction at $E_{\text{c.m.}} = 8.9$ MeV in inverse kinematics. The spectroscopic factor and ANC were derived based on distorted wave Born approximation (DWBA) analysis, and used to calculate the astrophysical S-factors and rates of $^{13}\text{N}(p, \gamma)^{14}\text{O}$ direct capture reaction at energies of astrophysical interest with the R-matrix approach. We have also computed the contribution from the resonant capture and the interference effect between resonant and direct capture. The total reaction rates are then used in the reaction network calculations at the typical density and temperature of novae environment.

II. MEASUREMENT OF THE $^{13}\text{N}(d, n)^{14}\text{O}$ ANGULAR DISTRIBUTION

The experiment was carried out using the secondary beam facility [19, 20] of the HI-13 tandem accelerator, Beijing. An 84 MeV ^{12}C primary beam from the tandem impinged on a 4.8 cm long deuterium gas cell at a pressure of 1.6 atm. The front and rear windows of the gas cell are Havar foils, each in thickness of 1.9 mg/cm². The ^{13}N ions were produced via the $^2\text{H}(^{12}\text{C}, ^{13}\text{N})n$ reaction. After the magnetic separation and focus with a dipole and a quadruple doublet, the secondary beam was further purified with a Wien filter. The 69 MeV ^{13}N secondary beam was then delivered with typical purity of 92%. The main contaminants were ^{12}C ions out of Rutherford scattering of the primary beam in the gas cell windows as

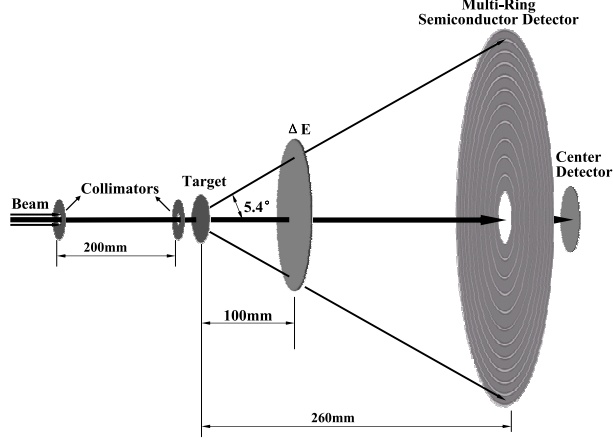


FIG. 1: Schematic layout of the experimental setup

well as on the beam tube. The ^{13}N beam was collimated with two apertures in diameter of 3 mm and directed onto a $(\text{CD}_2)_n$ target in thickness of 1.5 mg/cm^2 to study the $^2\text{H}(^{13}\text{N}, ^{14}\text{O})n$ reaction. The typical beam intensity and beam energy spread on the target were 1500 pps and 1.8 MeV FWHM for long-term measurement, respectively. A carbon target in thickness of 1.5 mg/cm^2 served as the background measurement.

The experimental setup is shown in Fig. 1. A $300 \mu\text{m}$ thick Multi-Ring Semiconductor Detector (MRSD) with center hole was used as a residue energy (E_r) detector which composed a $\Delta E - E_r$ counter telescope together with a $21.6 \mu\text{m}$ thick silicon ΔE detector and a $300 \mu\text{m}$ thick silicon center E_r detector. Such a detector configuration covered the laboratory angular range from 0° to 5.4° , and the corresponding angular range in the center-of-mass frame is from 0° to 66.5° . This setup also facilitates to precisely determine the accumulated quantity of incident ^{13}N because the ^{13}N themselves are recorded by the counter telescope simultaneously.

The accumulated quantity of incident ^{13}N is approximately 3.54×10^8 for the $(\text{CD}_2)_n$ target measurement, and 1.18×10^8 for background measurement with the carbon target. Fig. 2 (a) - (d) display the $\Delta E - E_r$ scatter plots for the first four rings, respectively. For the sake of saving CPU time in dealing with the experimental data, we set a cut line of $\Delta E = 19 \text{ MeV}$. All the events below the line are scaled down by a factor of 1000, and the ^{14}O events are not affected by this cut. The four two-dimension gates plotted in Fig. 2 (a) - (d) are the ^{14}O kinematics regions based on the Monte Carlo simulation, taking the beam spot size, energy spread, angular divergence and the target thickness into account. The ^{14}O events can be clearly identified through this figure. Fig. 3 displays the comparison of the

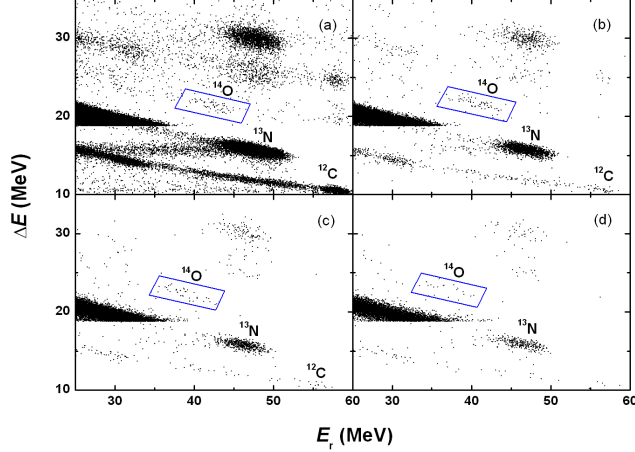


FIG. 2: (Color online) Scatter plots of ΔE vs. E_r for the $^{13}\text{N}(d, n)^{14}\text{O}$ reaction measurement with $(\text{CD}_2)_n$ target. (a) - (d) display the ΔE - E_r spectra for the first four rings of MRSD.

events from $(\text{CD}_2)_n$ target with the background from carbon target in the ^{14}O kinematics regions for the first four rings. The background events in the first ring of MRSD mainly come from the pileup of ^{12}C contaminants in the beam, they disappear in the outer rings. After the background subtraction, the angular distribution in center of mass frame for the forward angles is given in Fig. 4. The uncertainties of differential cross section mainly arise from the statistics, the assignment of ^{14}O kinematics regions, the uncertainties of the target thickness and the solid angle. The angular uncertainties include the random reaction point in the target, the angular uncertainty of the secondary beam, the angular straggling of ^{13}N and ^{14}O in the target and the ΔE detector. The total angular error for each ring is about 0.6 degree, less than the width of each ring.

III. DETERMINATION OF THE ^{14}O NUCLEAR ANC

The spins and parities of ^{13}N and ^{14}O (ground state) are $1/2^-$ and 0^+ , respectively. The cross section of the $^{13}\text{N}(d, n)^{14}\text{O}$ reaction is dominated by the s -wave proton transition to $1p_{1/2}$ orbit in ^{14}O ground state. If the reaction is peripheral, the differential cross section can be expressed as

$$\left(\frac{d\sigma}{d\Omega}\right)_{exp} = \left(\frac{C_d}{b_d}\right)^2 \left(\frac{C_{1,1/2}^{14\text{O}}}{b_{1,1/2}^{14\text{O}}}\right)^2 \sigma_{1,1/2}(\theta), \quad (1)$$

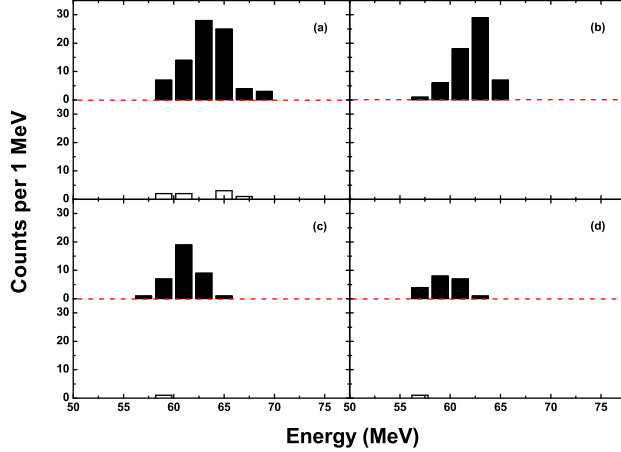


FIG. 3: (Color online) Comparison of total energy spectra between $(\text{CD}_2)_n$ and pure Carbon target. (a)-(d) represent the spectra for ring 1,2,3 and 4. The solid bar and the empty bar stand for the ^{14}O spectra from $(\text{CD}_2)_n$ target and carbon target, respectively.

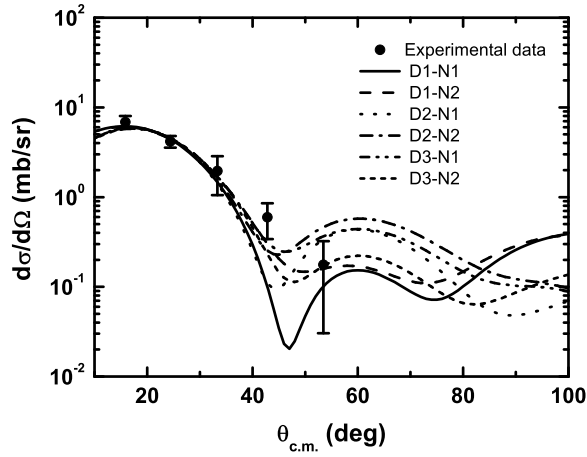


FIG. 4: The angular distribution of the $^{13}\text{N}(d,n)^{14}\text{O}$ reaction at $E_{c.m.} = 8.9$ MeV, together with DWBA calculations using different optical potential parameters.

where $(\frac{d\sigma}{d\Omega})_{exp}$ and $\sigma_{l,j}(\theta)$ denote the measured and theoretical differential cross sections respectively. $C_{1,1/2}^{14\text{O}}$ and C_d stand for the nuclear ANCs for the $^{14}\text{O} \rightarrow ^{13}\text{N} + p$ and $d \rightarrow n + p$ virtual decays, $b_{1,1/2}^{14\text{O}}$ and b_d being the single particle ANCs of the bound state protons in ^{14}O and deuteron. By knowing the value of C_d , the $C_{1,1/2}^{14\text{O}}$ can then be extracted by normalizing the theoretical differential cross sections to the experimental data by Eq. (1).

The DWBA code DWUCK [21] is used to compute the angular distribution. All the optical potential parameters for the entrance channel are taken from Ref. [22], the ones for the

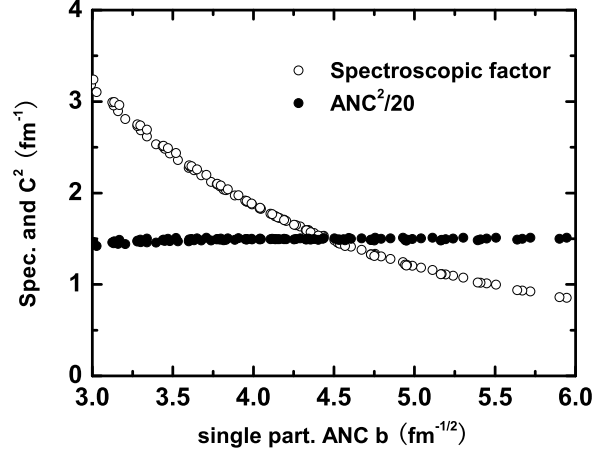


FIG. 5: Comparison of spectroscopic factors with the ANCs derived from the present experiment for different geometries of the Woods-Saxon potentials.

exit channel are from Refs. [22] and [23], respectively, these parameters are listed in Table I. In the present DWBA calculation, the differential cross sections at three forward angles are used to extract the ANC, and C_d is taken to be $0.872 \text{ fm}^{-1/2}$ from Ref. [24]. The normalized angular distributions from the six sets of optical potential parameters are also presented in Fig. 4, each curve corresponds to one nuclear ANC, $C_{1,3/2}^{14O}$, the spectroscopic factor is calculated with C^2/b^2 . The nuclear ANCs and the spectroscopic factors deduced from the present experimental data are listed in Table II, the average values of them are $5.42 \pm 0.48 \text{ fm}^{-1/2}$ and 1.88 ± 0.34 , respectively. The present ANC accords with the result extracted from the $^{14}\text{N}(^{13}\text{N}, ^{14}\text{O})^{13}\text{C}$ transfer reaction by Tang et al. [18], and the present spectroscopic factor is larger than the previous one (0.9) extracted from the total cross section of $^{13}\text{N}(d, n)^{14}\text{O}$ at lower energy [17]. The uncertainties of the nuclear ANC and the spectroscopic factor are mainly from the difference of the calculated angular distributions with different optical potentials, as well as the experimental errors. Since we do not measure the optical potential parameters and used six sets of potential parameters from the neighboring nuclei, the error bar of present work is a bit larger than that of Ref. [18]. Fig. 5 shows the comparison of the spectroscopic factors with ANCs of $^{14}\text{O} \rightarrow ^{13}\text{N} + p$ from the different geometry parameters of the Woods-Saxon potential for the single particle bound state (by changing the radius and diffuseness r_0 and a). One can see that the spectroscopic factors vary strikingly, while the ANCs are nearly a constant, thus indicating that the $^{13}\text{N}(d, n)^{14}\text{O}$ reaction at present energy is dominated by peripheral process.

TABLE I: Optical potential parameters used in DWBA calculations, where V , W are in MeV, r and a are in fm, the geometrical parameters of single particle bound state are set to be $r_0 = 1.25$ fm and $a = 0.65$ fm. D1, D2 and D3 correspond to the optical potentials for $d + {}^{13}\text{N}$, and N1, N2 represent the ones for $n + {}^{14}\text{O}$.

Channel	Entrance			Exit	
	D1	D2	D3	N1	N2
V_r	117.9	116.0	130.4	49.2	61.56
r_{0r}	0.81	1.0	0.9	1.2	1.14
a_r	1.07	0.8	0.9	0.65	0.57
W_V		4.13			
r_{wv}		1.0			
a_{wv}		0.8			
W_s	19.61	4.13	6.63	6.0	7.74
r_{0s}	1.84	2.0	1.90	1.2	1.14
a_s	0.35	0.6	0.56	0.47	0.5
V_{SO}		6.76		7.0	5.5
r_{0SO}		1.0		1.20	1.14
a_{SO}		0.8		0.65	0.8
r_{0c}	0.81	1.5	1.30		

IV. ASTROPHYSICAL S-FACTOR OF ${}^{13}\text{N}(p, \gamma){}^{14}\text{O}$

According to the traditional direct capture model [15, 16, 25], the direct capture of the ${}^{13}\text{N}(p, \gamma){}^{14}\text{O}$ reaction is believed to be dominated by the $E1$ transition from incoming s wave to bound p state. The direct capture cross section can be computed by

$$\sigma_{dc} = \frac{16\pi}{9} k_\gamma^3 \bar{e}^2 A_{ij} S_{l,j} \left| \int_0^\infty dr r^2 \varphi_{l_f}(r) \psi_{l_i}(r) \right|^2. \quad (2)$$

where $k_\gamma = \epsilon_\gamma/\hbar c$ is the wave number of the emitted γ -ray (of energy ϵ_γ) and $\bar{e} = eN/A$ is the $E1$ effective charge for protons, A_{ij} corresponds to the angular part depending on the initial and final angular momenta of the transition, $S_{l,j}$ is the spectroscopic factor of the configuration ${}^{14}\text{O} \rightarrow {}^{13}\text{N} + p$, $\varphi_{l_f}(r)$ is the bound state wave function of the relative

TABLE II: The ^{14}O nuclear ANC, $C_{1,1/2}^{14\text{O}}$, and spectroscopic factor, $S_{1,1/2}^{14\text{O}}$, deduced from the angular distribution of the $^{13}\text{N}(d, n)^{14}\text{O}$ reaction using the combination of optical potentials for the entrance and exit channels.

optical potentials	$C_{1,1/2}^{14\text{O}}$ ($\text{fm}^{-1/2}$)	$S_{1,1/2}^{14\text{O}}$
D1-N1	5.27 ± 0.42	1.77 ± 0.28
D1-N2	4.95 ± 0.17	1.56 ± 0.11
D2-N1	6.02 ± 0.61	2.31 ± 0.47
D2-N2	5.42 ± 0.29	1.87 ± 0.20
D3-N1	5.56 ± 0.27	1.97 ± 0.19
D3-N2	5.31 ± 0.19	1.80 ± 0.13
average	5.42 ± 0.48	1.88 ± 0.34

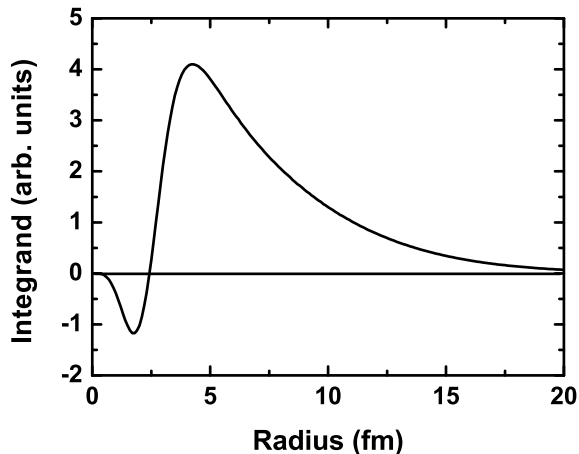


FIG. 6: The integrand of the $E1$ transition matrix element based on a single-particle model at resonant energy.

motion of $p+^{13}\text{N}$ in ^{14}O calculated in the Woods-Saxon potential, $\psi_{l_i}(r)$ is the optical model scattering wave function of the colliding proton and ^{13}N . If the spectroscopic factor $S_{l,j}$ is deduced from the $^{13}\text{N}(d, n)^{14}\text{O}$ transfer reaction, the $^{13}\text{N}(p, \gamma)^{14}\text{O}$ cross section can then be calculated by Eq. (2).

However, this is not the case here, as a result of the tight binding of the last proton in ^{14}O , the contribution to the $^{13}\text{N}(p, \gamma)^{14}\text{O}$ direct capture reaction at small r in Eq. (2) is important.

The integrand of the $E1$ transition matrix element at resonant energy is calculated based on a single-particle model, as shown in Fig. 6. One can see that the contribution at small r is of significance, the simple direct capture model may be not valid due to the many particle effects. In this case, the integral is very sensitive to the optical potential parameters and the spectroscopic factor required for Eq. (2) has significant uncertainties, as can be seen from Fig. 5.

In this work, we will use R-matrix method to avoid the above problems. For the radiative capture reaction $B + b \rightarrow A + \gamma$, the R-matrix radiative capture cross section to a state of nucleus A with a given spin J_f may be written as [26]

$$\sigma_{J_f} = \sum_{J_i} \sigma_{J_i J_f}, \quad (3)$$

$$\sigma_{J_i J_f} = \frac{\pi}{k^2} \frac{2J_i + 1}{(2J_b + 1)(2J_B + 1)} \sum_{l_i} |U_{l_i J_f J_i}|^2. \quad (4)$$

Here J_i is the total angular momentum of the colliding nuclei B and b in the initial state, J_b and J_B are the spins of nuclei b and B, and I , k , and l_i are their channel spin, wave number and orbital angular momentum in the initial state. $U_{l_i J_f J_i}$ is the transition amplitude from the initial continuum state (J_i, I, l_i) to the final bound state (J_f, I) . In the one-level, one-channel approximation, the resonant amplitude for the capture into the resonance with energy E_{R_n} and spin J_i , and subsequent decay into the bound state with the spin J_f can be expressed as

$$U_{l_i J_f J_i}^R = -i e^{i(\omega_{l_i} - \phi_{l_i})} \frac{[\Gamma_{b l_i}^{J_i}(E) \Gamma_{\gamma J_f}^{J_i}(E)]^{1/2}}{E - E_{R_n} + i \frac{\Gamma_{J_i}}{2}}. \quad (5)$$

Here we assume that the boundary parameter is equal to the shift function at resonance energy and ϕ_{l_i} is the hard-sphere phase shift in the l_i th partial wave,

$$\phi_{l_i} = \arctan \left[\frac{F_{l_i}(k, r_c)}{G_{l_i}(k, r_c)} \right], \quad (6)$$

where $F_{l_i}^2$ and $G_{l_i}^2$ are the regular and irregular Coulomb functions, r_c is the channel radius. The Coulomb phase factor ω_{l_i} is given by

$$\omega_{l_i} = \sum_{n=1}^{l_i} \arctan\left(\frac{\eta_i}{n}\right), \quad (7)$$

where η_i is the Sommerfeld parameter. $\Gamma_{b l_i}^{J_i}(E)$ is the observable partial width of the resonance in the channel $B + b$, $\Gamma_{\gamma J_f}^{J_i}(E)$ is the observable radiative width for the decay of

the given resonance into the bound state with the spin J_f , and $\Gamma_{J_i} \approx \sum_I \Gamma_{bIi}^{J_i}$ is the observable total width of the resonance level. The energy dependence of the partial widths is determined by

$$\Gamma_{bIi}^{J_i}(E) = \frac{P_i(E)}{P_i(E_{R_n})} \Gamma_{bIi}^{J_i}(E_{R_n}) \quad (8)$$

and

$$\Gamma_{\gamma J_f}^{J_i}(E) = \left(\frac{E + \varepsilon_f}{E_{R_n} + \varepsilon_f} \right)^{2L+1} \Gamma_{\gamma J_f}^{J_i}(E_{R_n}), \quad (9)$$

where $\Gamma_{bIi}^{J_i}(E_{R_n})$ and $\Gamma_{\gamma J_f}^{J_i}(E_{R_n})$ are the experimental partial and radiative widths, ε_f is the proton binding energy of the bound state in nucleus A , and L is the multipolarity of the gamma transition. The penetrability $P_i(E)$ is expressed as

$$P_i(E) = \frac{kr_c}{F_i^2(k, r_c) + G_i^2(k, r_c)}. \quad (10)$$

The nonresonant amplitude can be calculated by

$$\begin{aligned} U_{IiJ_fJ_i}^{NR} &= -(2)^{3/2} i^{l_i+L-l_f+1} e^{i(\omega_{l_i}-\phi_{l_i})} \frac{1}{\hbar k} \mu_{Bb}^{L+1/2} \\ &\times \left[\frac{Z_b e}{m_b^L} + (-1)^L \frac{Z_B e}{m_B^L} \right] \sqrt{\frac{(L+1)(2L+1)}{L}} \\ &\times \frac{1}{(2L+1)!!} (k_\gamma r_c)^{L+1/2} C_{J_f I_i} F_{l_i}(k, r_c) \\ &\times G_{l_i}(k, r_c) W_{l_f}(2\kappa r_c) \sqrt{P_i(l_i 0 L 0 | l_f 0)} \\ &\times U(L l_f J_i I; l_i J_f) J'_L(l_i l_f), \end{aligned} \quad (11)$$

where

$$\begin{aligned} J'_L(l_i l_f) &= \frac{1}{r_c^{L+1}} \int_{r_c}^{\infty} dr r \frac{W_{l_f}(2\kappa r)}{W_{l_f}(2\kappa r_c)} \left[\frac{F_{l_i}(k, r)}{F_{l_i}(k, r_c)} \right. \\ &\quad \left. - \frac{G_{l_i}(k, r)}{G_{l_i}(k, r_c)} \right]. \end{aligned} \quad (12)$$

Here, $W_l(2\kappa r)$ is the Whittaker hypergeometric function, $\kappa = \sqrt{2\mu_{Bb}\varepsilon_f}$ and l_f are the wave number and relative orbital angular momentum of the bound state, and $k_\gamma = (E + \varepsilon_f)/\hbar c$ is the wave number of the emitted photon.

The non-resonant amplitude contains the radial integral ranging only from the channel radius r_c to infinity since the internal contribution is contained within the resonant part. Furthermore, the R-matrix boundary condition at the channel radius r_c implies that the scattering of particles in the initial state is given by the hard sphere phase. Hence, the

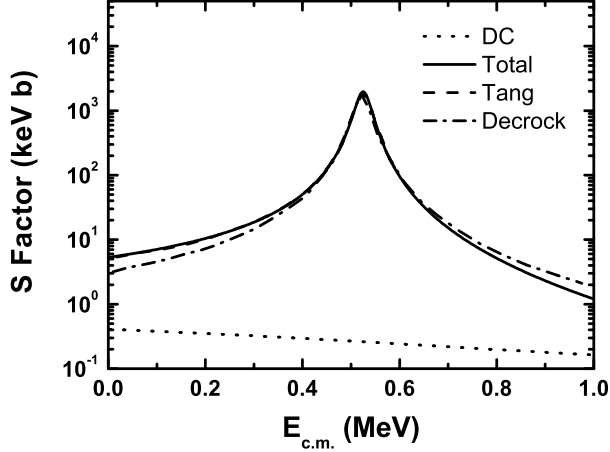


FIG. 7: Astrophysical S-factors as a function of $E_{c.m.}$ for the $^{13}\text{N}(p, \gamma)^{14}\text{O}$ reaction. The dotted line is the contributions from the direct proton capture. The solid, dashed, and dashed-dotted lines indicate the total S-factors from the present work, Refs. [18] and [17], respectively.

problems related to the interior contribution and the choice of incident channel optical parameters do not occur. Therefore, the direct capture cross section only depends on the ANC and the channel radius r_c .

The astrophysical S-factor is related to the cross section by

$$S(E) = E\sigma(E) \exp(E_G/E)^{1/2}, \quad (13)$$

where the Gamow energy $E_G = 0.978Z_1^2Z_2^2\mu$ MeV, μ is the reduced mass of the system. According to the experimental ANC ($5.42 \pm 0.48 \text{ fm}^{-1/2}$) from the present work, and the resonance parameters ($E_R = 527.9 \pm 1.7$ keV, $\Gamma_{tot}(E_R) = 37.3 \pm 0.9$ keV, and $\Gamma_\gamma(E_R) = 3.36 \pm 0.72$ eV) from Ref. [8], the S-factors for direct and resonant captures can be then derived, as demonstrated in Fig. 7.

Since the incoming angular momentum (*s*-wave) and the multipolarity ($E1$) of the direct and resonant capture γ -radiation are identical, there is an interference between the direct and the resonant captures. In this case, the total S-factor is calculated with [15]

$$S_{tot}(E) = S_{dc}(E) + S_{res}(E) \pm 2[S_{dc}(E)S_{res}(E)]^{1/2} \cos(\delta), \quad (14)$$

where δ is the resonance phase shift, which can be given by

$$\delta = \arctan\left[\frac{\Gamma_p(E)}{2(E - E_r)}\right]. \quad (15)$$

TABLE III: The present total reaction rate for $^{13}\text{N}(p, \gamma)^{14}\text{O}$, $N_A \langle \sigma v \rangle$ ($\text{cm}^3 \text{mole}^{-1} \text{s}^{-1}$), as a function of temperature, together with the previous results.

T_9	Present work	Ref. [Tang]	NACRE
0.01	4.44×10^{-22}	4.18×10^{-22}	2.01×10^{-22}
0.02	6.02×10^{-16}	5.72×10^{-16}	2.78×10^{-16}
0.03	5.60×10^{-13}	5.35×10^{-13}	2.63×10^{-13}
0.04	4.16×10^{-11}	3.98×10^{-11}	1.99×10^{-11}
0.05	8.89×10^{-10}	8.53×10^{-10}	4.34×10^{-10}
0.06	9.19×10^{-9}	8.84×10^{-9}	4.58×10^{-9}
0.07	5.94×10^{-8}	5.72×10^{-8}	3.02×10^{-8}
0.08	2.77×10^{-7}	2.67×10^{-7}	1.44×10^{-7}
0.09	1.02×10^{-6}	9.86×10^{-7}	5.43×10^{-7}
0.1	3.15×10^{-6}	3.04×10^{-6}	1.71×10^{-6}
0.13	4.41×10^{-5}	4.27×10^{-5}	2.56×10^{-5}
0.17	5.32×10^{-4}	5.16×10^{-4}	3.34×10^{-4}
0.21	3.34×10^{-3}	3.24×10^{-3}	2.22×10^{-3}
0.25	1.44×10^{-2}	1.39×10^{-2}	9.85×10^{-3}
0.29	5.00×10^{-2}	4.84×10^{-2}	3.47×10^{-2}
0.33	1.56×10^{-1}	1.51×10^{-1}	1.11×10^{-1}
0.37	4.56×10^{-1}	4.41×10^{-1}	3.41×10^{-1}
0.41	1.24×10^0	1.20×10^0	9.91×10^{-1}
0.45	3.07×10^0	2.98×10^0	2.60×10^0
0.49	6.87×10^0	6.69×10^0	6.09×10^0
0.53	1.39×10^1	1.36×10^1	1.28×10^1
0.57	2.59×10^1	2.54×10^1	2.44×10^1
0.61	4.46×10^1	4.38×10^1	4.27×10^1
0.65	7.20×10^1	7.09×10^1	6.99×10^1
0.69	1.10×10^2	1.09×10^2	1.08×10^2
0.73	1.60×10^2	1.58×10^2	1.58×10^2
0.77	2.23×10^2	2.22×10^2	2.22×10^2
0.81	3.01×10^2	2.99×10^2	3.01×10^2
0.85	3.94×10^2	3.92×10^2	3.95×10^2
0.89	5.02×10^2	5.00×10^2	5.04×10^2
0.93	6.26×10^2	6.23×10^2	6.30×10^2
0.97	7.64×10^2	7.59×10^2	7.70×10^2

Generally, the sign of the interference in Eq. (14) has to be determined experimentally. However, it is possible sometimes to infer this sign. The interference between the resonant and direct capture contributions is constructive below the resonance energy and destructive above it, which has been observed from the isospin analog $^{13}\text{C}(p, \gamma)^{14}\text{N}^*$ (2.31 MeV) reaction [17]. Recently, Tang et al. deduced constructive interference below the resonance using an R-matrix method [18]. Based on this interference pattern, the present total S-factor is then obtained. Fig. 7 shows the comparison of total S-factors from the present work, Refs. [18] and [17]. Our updated total S-factors are about 40% higher than the previous ones in Ref. [17] at low energies and is in good agreement with that in Ref. [18].

V. THE ASTROPHYSICAL REACTION RATE

The astrophysical reaction rate of $^{13}\text{N}(p, \gamma)^{14}\text{O}$ is calculated with

$$N_A \langle \sigma v \rangle = N_A \left(\frac{8}{\pi \mu} \right)^{1/2} \frac{1}{(kT)^{3/2}} \int_0^\infty S(E) \times \exp \left[- \left(\frac{E_G}{E} \right)^{1/2} - \frac{E}{kT} \right] dE, \quad (16)$$

where N_A is Avogadro constant. The updated rates are listed in Table III, together with the previous ones from Ref. [18] and NACRE's compilation. The results from the three works agree with each other within a factor of 2 at low temperature of $T < 0.2$ GK and are almost identical at higher temperature of $T > 0.7$ GK.

The present total reaction rates as a function of temperature T_9 (in unit of 10^9 K) are fitted with an expression used in the astrophysical reaction rate library REACLIB [27],

$$N_A \langle \sigma v \rangle = \exp[-5.2635 + 0.0364T_9^{-1} - 21.5656T_9^{-1/3} + 36.0575T_9^{1/3} - 4.9432T_9 + 0.3937T_9^{5/3} - 9.7467 \ln(T_9)] + \exp[108.6965 + 0.6657T_9^{-1} - 47.9051T_9^{-1/3} - 59.4921T_9^{1/3} + 5.0145T_9 - 0.2488T_9^{5/3} + 4.4288 \ln(T_9)]. \quad (17)$$

The fitting errors are less than 5% in the range from $T_9 = 0.01$ to $T_9 = 10$.

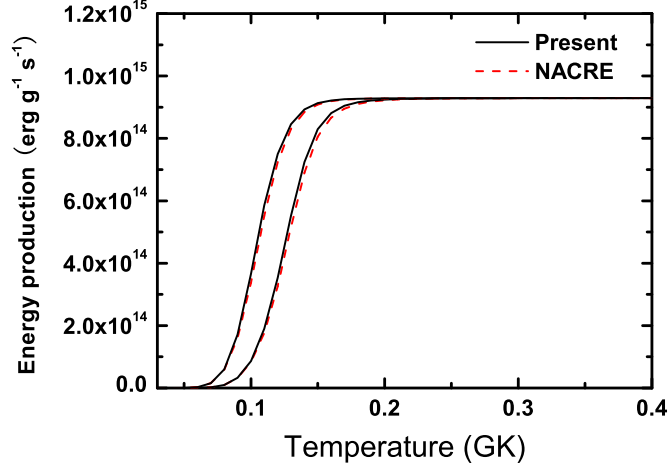


FIG. 8: (Color online) Energy production rates of the CNO and hot CNO cycles at $\rho = 500$ (right) and 5000 (left) g/cm^3 for novae with the update $^{13}N(p, \gamma)^{14}O$ reaction rates from present work and NACRE's compilation.

For a given density ρ , the reaction network equations and the energy source equation have the following forms:

$$\begin{aligned} \dot{Y}_i - F(Y_j, T) &= 0 \\ \dot{\epsilon} + \sum_i N_A M_i c^2 \dot{Y}_i &= 0 \end{aligned} \quad (18)$$

where Y_i are the nuclear abundances, $\dot{\epsilon}$ is the energy production rate per unit mass, $i, j = 1, 2, \dots, N$, and N is the number of nuclear species. F denotes nonlinear functions of the arguments, and $M_i c^2$ is the rest mass energy of species i in MeV. At equilibrium, the abundances do not change with the time approximately, i.e., $\dot{Y}_i \simeq 0$, the energy production rate can then be calculated by substituting the reaction rates into Eq. (18). Fig. 8 shows the energy productions of CNO and hot CNO cycles at density $\rho = 500$ and $5000 g/cm^3$ for novae with the $^{13}N(p, \gamma)^{14}O$ reaction rates from present work and NACRE's compilation. One can see that the hot CNO cycle would begin to run earlier and produce more energy with our updated $^{13}N(p, \gamma)^{14}O$ reaction rates. The present result shows that about 5% of additional energy could be produced at the temperature range from 0.07 to 0.15 GK, which implies that the evaluation of a nova may be affected.

VI. SUMMARY

In summary, $^{13}\text{N}(p, \gamma)^{14}\text{O}$ is one of the key reactions which trigger the onset of the hot CNO cycle. We have measured the angular distribution of the $^{13}\text{N}(d, n)^{14}\text{O}$ reaction at $E_{c.m.} = 8.9$ MeV, and deduced the nuclear ANC and spectroscopic factor for the ^{14}O ground state. The astrophysical S-factors and reaction rates for $^{13}\text{N}(p, \gamma)^{14}\text{O}$ are then extracted with the R-matrix approach. Our result is in good agreement with that from the $^{14}\text{N} (^{13}\text{N}, ^{14}\text{O})^{13}\text{C}$ transfer reaction by Tang et al. [18]. The reaction network calculations have been performed with the updated $^{13}\text{N}(p, \gamma)^{14}\text{O}$ reaction rates, the result shows that 5% additional energy could be generated through the CNO and hot CNO cycles at the typical densities and temperature range from 0.07 to 0.15 GK for the novae, this may affect the evaluation of novae.

Acknowledgments

This work was supported by the National Natural Science Foundation of China under Grant Nos. 10375096, 10575136 and 10405035.

-
- [1] G. J. Mathews and F. S. Dietrich, *The Astrophys. J.* **287**, 969 (1984).
 - [2] M. Wiescher, J. Görres, and H. Schatz, *J. Phys. G* **25**, R133 (1999).
 - [3] P. Decrock, T. Delbar, P. Duhamel, W. Galster, M. Huyse, P. Leleus, I. Licot, E. Liénard, P. Lipnik, M. Loiselet, et al., *Phys. Rev. Lett.* **67**, 808 (1991).
 - [4] T. Delbar, W. Galster, P. Leleux, I. Licot, E. Liénard, P. Lipnik, M. Loiselet, C. Michotte, G. Ryckewaert, J. Vervier, et al., *Phys. Rev. C* **48**, 3088 (1993).
 - [5] T. E. Chupp, R. T. Kouzes, A. B. McDonald, P. D. Parker, T. F. Wang, and A. Howard, *Phys. Rev. C* **31**, 1023 (1985).
 - [6] P. B. Fernandez, E. G. Adelberger, and A. Garcia, *Phys. Rev. C* **40**, 1887 (1989).
 - [7] M. S. Smith, P. Magnus, K. I. Hahn, R. M. Curley, P. D. Parker, T. F. Wang, K. E. Rehm, P. B. Fernandez, S. J. Sanders, A. Garcia, et al., *Phys. Rev. C* **47**, 2740 (1993).
 - [8] P. V. Magnus, E. G. Adelberger, and A. Garcia, *Phys. Rev. C* **49**, R1755 (1994).
 - [9] G. Bauer and H. Rebel, *J. Phys. G* **20**, 1 (1994).

- [10] T. Motobayashi, T. Takei, S. Kox, C. Perrin, F. Merchez, D. Rebreyend, K. Ieki, H. Murakami, Y. Ando, N. Iwasa, et al., *Phys. Lett. B* **264**, 259 (1991).
- [11] J. Kiener, A. Lefebvre, P. Aguer, C. O. Bacri, R. Bimbot, G. Bogaert, B. Borderie, F. Clapier, A. Coc, D. Disdier, et al., *Nucl. Phys. A* **552**, 66 (1993).
- [12] F. C. Barker, *Austr. J. Phys.* **38**, 657 (1985).
- [13] C. Funck and K. Langanke, *Nucl. Phys. A* **464**, 90 (1987).
- [14] P. Descouvemont and D. Baye, *Nucl. Phys. A* **500**, 155 (1989).
- [15] C. Rolfs, *Nucl. Phys. A* **217**, 29 (1973).
- [16] R. F. Christy and I. Duck, *Nucl. Phys. A* **24**, 89 (1961).
- [17] P. Decrock, M. Gaelens, M. Huyse, G. Reusen, G. Vancracynest, P. V. Duppen, J. Wauters, T. Delbar, W. Galster, P. Leleux, et al., *Phys. Rev. C* **48**, 2057 (1993).
- [18] X. Tang, A. Azhari, C. Fu, C. A. Gagliardi, A. M. Mukhamedzhanov, F. Pirlepesov, L. Trache, R. Tribble, V. Burjan, V. Kroha, et al., *Phys. Rev. C* **69**, 055807 (2004).
- [19] X. Bai, W. liu, J. Qin, Z. Li, S. Zhou, A. Li, Y. Wang, Y. Cheng, and W. Zhao, *Nucl. Phys. A* **588**, 273c (1995).
- [20] W. P. Liu, Z. H. Li, X. X. Bai, Y. B. Wang, G. Lian, S. Zeng, S. Q. Yan, B. X. Wang, Z. X. Zhao, T. J. Zhang, et al., *Nucl. Instrum. Methods Phys. Res. B* **204**, 62 (2003).
- [21] P. D. Kunz, *Computer code DWUCK* (unpublished).
- [22] C. M. Perey and F. G. Perey, *Atomic data and nuclear data tables* **17**, 1 (1976).
- [23] B. A. Watson, P. P. Singh, and R. E. Segel, *Phys. Rev.* **182**, 977 (1969).
- [24] L. D. Blokhintsev, I. Borbely, and E. I. Dolinskii, *Sov. J. Part. Nucl.* **8**, 485 (1977).
- [25] Z. H. Li, W. P. Liu, X. X. Bai, B. Guo, G. Lian, S. Q. Yan, B. X. Wang, S. Zeng, Y. Lu, J. Su, et al., *Phys. Rev. C* **71**, 052801(R) (2005).
- [26] F. C. Barker and T. Kajino, *Aust. J. Phys.* **44**, 693 (1991).
- [27] F. K. Thielemann, M. Arnould, and J. Truran, *Advances in Nuclear Astrophysics, edited by E. Vangioni-Flam et al.* (Gif-sur-Yvette: Editions Frontieres, 1987).